Received: 7 February 2023 | Revised: 19 March 2023 | Accepted: 21 March 2023

DOI: 10.1111/cbdd.14238

RESEARCH ARTICLE

WILEY

# Exploration of a new class of monoamine oxidase B inhibitors by assembling benzyloxy pharmacophore on halogenated chalcones

**Ashutosh Kumar Singh**[1] | **Seong-Min Kim**[2] | **Jong Min Oh**[2] | **Mohamed A. Abdelgawad**[3,4] | **Mohammed M. Ghoneim**[5] | **T. M. Rangarajan**[6] | **Sunil Kumar**[1] | **Sachithra Thazhathuveedu Sudevan**[1] | **Daniela Trisciuzzi**[7] | **Orazio Nicolotti**[7] | **Hoon Kim**[2] | **Bijo Mathew**[1]

[1]Department of Pharmaceutical Chemistry, Amrita School of Pharmacy, Amrita Vishwa Vidyapeetham, Kochi, India

[2]Department of Pharmacy, and Research Institute of Life Pharmaceutical Sciences, Sunchon National University, Suncheon, Korea

[3]Department of Pharmaceutical Chemistry, College of Pharmacy, Jouf University, Sakaka, Saudi Arabia

[4]Department of Pharmaceutical Organic Chemistry, Faculty of Pharmacy, Beni-Suef University, Beni-Suef, Egypt

[5]Department of Pharmacy Practice, College of Pharmacy, AlMaarefa University, Ad Diriyah, Saudi Arabia

[6]Department of Chemistry, Sri Venketeswara College, University of Delhi, New Delhi, India

[7]Dipartimento di Farmacia—Scienze del Farmaco, Università degli Studi di Bari "Aldo Moro", Bari, Italy

**Correspondence**
Hoon Kim, Department of Pharmacy, and Research Institute of Life Pharmaceutical Sciences, Sunchon National University, Suncheon 57922, Korea.
Email: hoon@sunchon.ac.kr

Bijo Mathew, Department of Pharmaceutical Chemistry, Amrita School of Pharmacy, Amrita Vishwa Vidyapeetham, AIMS Health Sciences Campus, Kochi 682 041, India.
Email: bijomathew@aims.amrita.edu and bijovilaventgu@gmail.com

**Funding information**
Amrita Vishwa Vidyapeetham University, Grant/Award Number: K-PHAR-20-628

## Abstract

Eight derivatives of benzyloxy-derived halogenated chalcones (**BB1-BB8**) were synthesized and tested for their ability to inhibit monoamine oxidases (MAOs). MAO-A was less efficiently inhibited by all compounds than MAO-B. Additionally, the majority of the compounds displayed significant MAO-B inhibitory activities at 1 μM with residual activities of less than 50%. With an $IC_{50}$ value of 0.062 μM, compound **BB4** was the most effective in inhibiting MAO-B, followed by compound **BB2** ($IC_{50}$ = 0.093 μM). The lead molecules showed good activity than the reference MAO-B inhibitors (Lazabemide $IC_{50}$ = 0.11 μM and Pargyline Pargyline $IC_{50}$ = 0.14). The high selectivity index (SI) values for MAO-B were observed in compounds **BB2** and **BB4** (430.108 and 645.161, respectively). Kinetics and reversibility experiments revealed that **BB2** and **BB4** were reversible competitive MAO-B inhibitors with $K_i$ values of 0.030 ± 0.014 and 0.011 ± 0.005 μM, respectively. Swiss target prediction confirmed the high probability in the targets of MAO-B for both compounds. Hypothetical binding mode revealed that the **BB2** or **BB4** is similarly oriented to the binding cavity of MAO-B. Based on the modelling results, **BB4** showed a stable confirmation during the dynamic simulation. From these results, it was concluded that **BB2** and **BB4** were potent selective reversible MAO-B inhibitors and they can be considered drug candidates for treating related neurodegenerative diseases such as Parkinson's disease.

Ashutosh Kumar Singh and Seong-Min Kim authors contributed equally to this work.

  

**KEYWORDS**
benzyloxy chalcones, docking simulation, inhibition kinetics, reversibility, selective MAO-B inhibitor

## 1 | INTRODUCTION

Parkinson's disease (PD) is a prevalent degenerative neurological ailment that now affects about 2% of individuals over the age of 60 (de Lau & Breteler, 2006). Dopaminergic cell apoptosis in the substantia nigra causes striatal dopamine deficit, which results in motoric disorders such as bradykinesia, rest tremor, and stiffness. Non-motor manifestations including autonomic dysfunction, insomnia, stress, anxiety, and cognitive abnormalities can be devastating and can arise at any stage of PD (Elmer & Bertoni, 2008). Therapies that control the dopamine system, either by giving or enhancing dopaminergic function (dopamine agonists), exogenous dopamine (levodopa), or intervening degradation of dopamine as monoamine oxidase (MAO)-B inhibitors have proven to be the most helpful for PD motor symptoms. MAO-B inhibitor is useful as a stand-alone treatment for initial PD and as an adjunct treatment on levodopa in terminal PD. However, there is currently no neuroprotective medication that can stop the progression of PD (Carradori & Silvestri, 2015; Robakis & Fahn, 2015).

MAO enzymes are the primary digesting enzymes accountable for the destruction of a variety of biogenic amines linked to a variety of central nervous system (CNS) cognitive processes (Finberg & Rabey, 2016). MAOs are divided into two categories based on their structure, substrate selectivity, biological roles, and catalytic mechanism, i.e., MAO-A and MAO-B. The key intermediate products generated through MAO-catalyzed oxidative deamination are ammonia, aldehyde, and hydrogen peroxide. These can result in serious problems such as astrocyte enlargement, unbalanced neurotransmission, neuronal death, and mitochondrial malfunction (Schapira, 2011). These toxic metabolic end products can eventually lead to a wide range of neurodegenerative conditions, including PD and Alzheimer's disease (AD) (Tan et al., 2022). In order to boost synaptic dopamine by preventing its breakdown, MAO-B inhibitors are employed in the symptomatic treatment of PD. Selegiline is a preferential/irreversible inhibitor of MAO-B used in conjunction with L-DOPA, which is regarded as a safer treatment for PD. The most recent exploration also showed that powerful and dual-targeted reversible MAO-B inhibitors can reduce amyloid protein concentrations in AD-related neurons (Fabbrini et al., 2012). Safinamide, the prime selective reversible inhibitor in regard to MAO-B, licensed through USFDA for PD therapy, combined with levodopa, showed potential neuroprotective benefits in 1-methyl-4-phenyl-1,2,3,6-tetr ahydropyridine (MPTP)-treated mice in 2017 (Tripathi & Ayyannan, 2019).

Although the two isoforms of MAOs share almost 70% of the amino acid sequence, they differ in various ways, including amino acid sequence, three-dimensional shape of the binding cavity, and inhibitor selectivity (Edmondson, 2004). The functioning site of MAO-A contains a lone hydrophobic pocket into which substrate binds, whereas the active site of MAO-B subsists with two cavities, a substrate pocket and a tiny entry cavity. The MAO-B isoform's substrate cavity links through FAD cofactors, whereas the entry pocket is located on the protein's exterior surface (Abell & Kwan, 2001; Shih & Chen, 2004). Ile335 in MAO-A and Tyr326 in MAO-B are another two variations in the substrate-binding areas of both enzymes that subsidize their selectiveness. MAO inhibitors are used to treat a variety of conditions, including high blood pressure and anxiety, schizophrenia, and depression (Carradori & Silvestri, 2015).

Chalcones are significant precursors for natural flavonoid production and are employed in a variety of synthetic modifications for a variety of enzyme targets (Zhuang et al., 2017). It is a simple chemical structure with a small α,β-unsaturated ketone linker. The existence of this olefinic connection with carbonyl functional group and both *cis* and *trans* isomers are obligated for variety of pharmacological activity (Mathew et al., 2019). Chalcones having various substitutions at different locations were investigated for treating a wide range of pathological illnesses such as inflammation, cancer, cardiac problems, malaria, diabetes, and oxidative stress, and infections such as viral and bacterial (Annapurna et al., 2012; Cheng et al., 2020; de Souza et al., 2021; Elkhalifa et al., 2021; Kontogiorgis et al., 2008; Sousa et al., 2021; Xu et al., 2019). They also have a broad range of CNS activities, including acetylcholinesterase (AChE) and butyrylcholinesterase (BChE) inhibition, anti-depressant, MAO inhibition, and anti-Alzheimer characteristics (Kontogiorgis et al., 2008). Many researches have been conducted to investigate the significance of electron-donating and electron-withdrawing groups on the different locations on chalcone **A** and **B** rings for MAO-B inhibition. The capacity of chalcone scaffold to function on the CNS is reliant on its low polar surface area, which allows for blood–brain barrier (BBB)

penetration (Guglielmi et al., 2020; Kumar et al., 2021; Mathew et al., 2015; Mathew et al., 2022; Mellado et al., 2019; Parambi et al., 2019).

The benzyloxy unit is usually a benzyl group with an oxygen atom and often acts as a shielding group in synthetic chemistry. Because of their significantly greater reactivity, benzylic -CH linkages have relatively low dissociation energy; however, oxygen, as an electronegative element, has a substantial bond dissociation energy, culminating in a sturdy binding. The insertion of the benzyloxy group to organic compounds of therapeutic relevance had also manifested in a significant shift in bioactivities (Al-Salahi et al., 2011). The moieties associated to the benzyloxy group, such as indolalkylamines, nitrostyrene, safinamide, oxadiazolones, benzofurans, benzoquinones, coumarins, caffeines, indoles, tetralones, chromanone and chromones analogues, exhibit substantial MAO-B inhibiting activities. When acting as a MAO inhibitor, the benzyloxy group attached to some frameworks reinforced the importance of a conformationally flexible terminus phenyl, which was then strengthened by adding a conformationally pliable -$CH_2O$- bridge (Chimenti et al., 2009; Knez et al., 2022; Mostert et al., 2017; Pérez et al., 1999; Rao et al., 2021; Rullo et al., 2019; Sudevan, Rangarajan, et al., 2022).

In 2007, Binda et al. investigated safinamide a benzyloxy-derived class of drug using the inhibition of human-recombinant MAO-B with non-covalent interactions. A non-covalent binding relationship with the enzyme was discovered in the human MAO-B crystalline framework, a desirable characteristic to reduce unwanted side effects like target disruptions and prolonged duration of action (Binda et al., 2007; Joy et al., 2018). It is generally recognized that halogens have a role in MAO inhibition since they are present in FDA-approved MAO inhibitors such moclobemide, clorgyline, safinamide, and lazabemide. According to the research, more than 40% of medications under FDA-approved or clinical studies are halogenated. The stabilizing impact of halogen bonding in the enzyme's inhibitor-binding cavity (IBC) led to an improvement in MAO-B selectivity when halogens were added to several types of MAO inhibitors (Bolasco et al., 2010; Fang et al., 2019; Mathew et al., 2020). Most of the currently used MAO inhibitors cause significant adverse effects such as hypertension, constipation, nausea, and others due to permanent inactivation of the enzyme, highlighting the need for new therapeutic options (Tripathi & Ayyannan, 2019). There are only few reversible medications available. According to several recent research, medicines for MAO-B suppression should have one or more hydrophobic rings in order to attach readily to the target hydrophobic pocket (Tripathi & Ayyannan, 2019). Our design strategy (Figure 1) aims to combine a benzyloxy unit to the halogenated chalcones and evaluate their inhibition studies of MAOs.

## 2 | MATERIALS AND METHODS

### 2.1 | Synthesis

A mixture consisting of various *para*-substituted acetophenones (0.001 M), 30 mL ethanol and 15 mL of 40% KOH was stirred in a magnetic stirrer for 25–35 min. Following that, 0.001 M of 4-*para/ortho* benzyloxy-substituted benzaldehyde was progressively added while being agitated constantly for 20–28 h. The substance was transferred to an ice-crushed beaker, then precipitate was completely filtered with water, dried, and recrystallized with ethanol. Thin layer chromatography was used to keep track of the reaction's progress (hexane: ethyl acetate = 6:1).

#### 2.1.1 | (2Z)-3-[4-(benzyloxy)phenyl]-1-phenylprop-2-en-1-one (**BB1**)

$^1$H NMR (500 MHz, Chloroform-*d*): δ 8.00 (d, 2H), 7.78 (d, $J$ = 15.6 Hz, 1H), 7.62–7.54 (m, 3H), 7.52–7.38 (m, 7H), 7.36–7.32 (m, 1H), 7.04–6.99 (m, 2H), 5.11 (s, 2H); $^{13}$C NMR (125 MHz, $CDCl_3$) δ 190.63, 160.88, 144.68, 138.53, 136.43, 132.60, 130.27, 128.70, 128.60, 128.45, 128.20, 127.90, 127.50, 119.96, 115.34, 70.15. Molecular formula $C_{22}H_{18}O_2$ (HRMS) Calculated = 314.3771, Observed = 314.3798.

#### 2.1.2 | (2Z)-3-[4-(benzyloxy)phenyl]-1-(4-chlorophenyl)prop-2-en-1-one (**BB2**)

$^1$H NMR (500 MHz, Chloroform-*d*) δ 7.96–7.91 (m, 2H), 7.79–7.76 (d, $J$ = 15.6 Hz, 1H), 7.68–7.58 (m, 2H), 7.47–7.45 (m, 2H), 7.44–7.34 (m, 6H), 7.01–7.00 (m, 2H), 5.11 (d, $J$ = 3.7 Hz, 2H); $^{13}$C NMR (126 MHz, $CDCl_3$) δ 189.23, 161.03, 145.19, 138.99, 136.82, 136.37, 130.36, 129.85, 128.89, 128.70, 128.22, 127.49, 119.32, 115.38, 70.16. Molecular formula $C_{22}H_{17}O_2Cl$ (HRMS) Calculated = 348.8221, Observed = 348.8198.

#### 2.1.3 | (2Z)-3-[4-(benzyloxy)phenyl]-1-(4-fluorophenyl)prop-2-en-1-one (**BB3**)

$^1$H NMR (500 MHz, Chloroform-*d*) δ 8.06–8.02 (m, 2H), 7.78 (d, $J$ = 15.6 Hz, 1H), 7.62–7.57 (m, 2H), 7.43–7.38 (m, 5H), 7.19–7.10 (m, 3H), 7.03–6.99 (m, 2H), 5.12 (s, 2H). $^{13}$C NMR (125 MHz, $CDCl_3$) δ 188.88, 174.34, 160.96, 144.87, 136.40, 131.02, 130.95, 130.30, 128.70, 128.22, 127.49, 119.41, 115.76, 115.59, 115.36, 70.16. Molecular formula $C_{22}H_{17}O_2F$ (HRMS) Calculated = 332.3675, Observed = 332.3697.

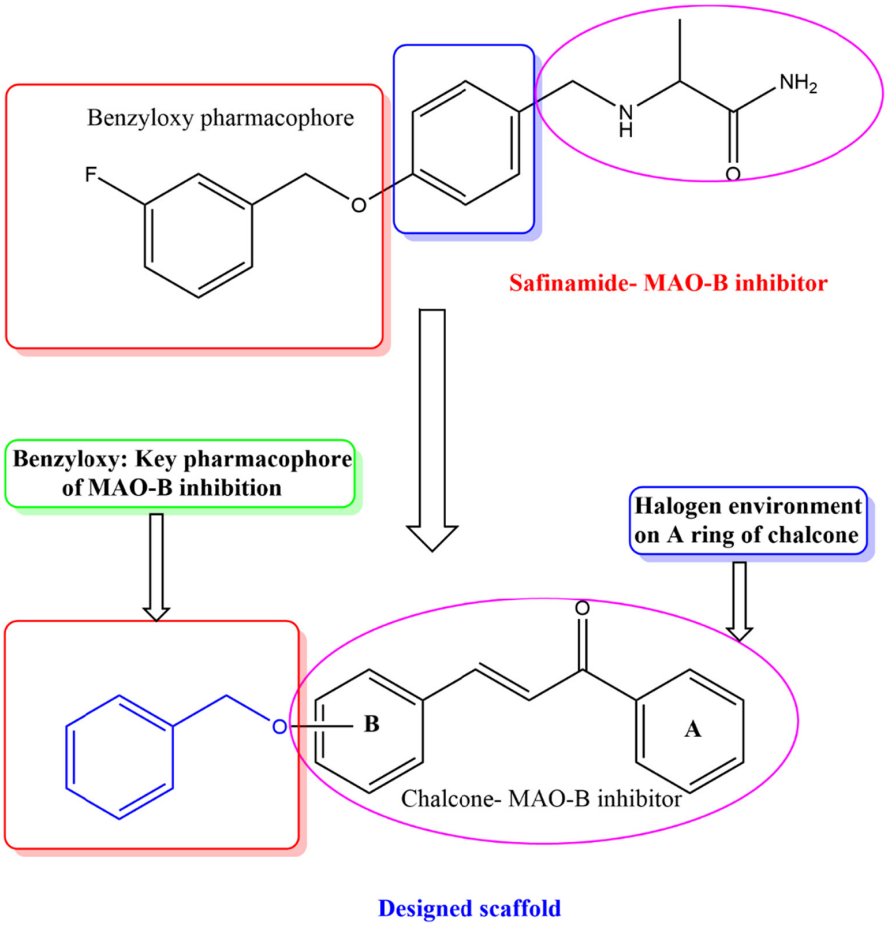


**FIGURE 1** Design strategy of benzyloxy-derived MAO-B inhibitors.

### 2.1.4 | (2Z)-3-[4-(benzyloxy)phenyl]-1-(4-bromophenyl)prop-2-en-1-one (**BB4**)

$^1$H NMR (500 MHz, Chloroform-*d*) δ 7.90–7.83 (m, 2H), 7.78 (d, *J* = 15.6 Hz, 1H), 7.67–7.53 (m, 4H), 7.46–7.29 (m, 6H), 7.04–6.96 (m, 2H), 5.11 (s, 2H).$^{13}$C NMR (125 MHz, $CDCl_3$) δ 189.41, 161.05, 145.25, 137.24, 136.37, 131.88, 130.38, 129.98, 128.71, 128.23, 127.65, 127.49, 119.29, 115.39, 70.16. Molecular formula $C_{22}H_{17}O_2Br$ (HRMS) Calculated = 393.2731, Observed = 393.2698.

### 2.1.5 | (2Z)-3-[2-(benzyloxy)phenyl]-1-phenylprop-2-en-1-one (**BB5**)

$^1$H NMR (500 MHz, Chloroform-*d*) δ 8.06 (d, *J* = 15.9 Hz, 1H), 7.88–7.81 (m, 2H), 7.75 (d, *J* = 15.8 Hz, 1H), 7.61 (dd, *J* = 7.7, 1.7 Hz, 1H), 7.57–7.47 (m, 3H), 7.41 (dd, *J* = 11.1, 5.6, 3.0 Hz, 5H), 7.37–7.32 (m, 1H), 7.25 (s, 1H), 7.02 (t, *J* = 7.5 Hz, 2H), 5.17 (s, 2H); $^{13}$C NMR (126 MHz, $CDCl_3$) δ 191.05, 158.24, 140.88, 138.39, 136.44, 132.48, 131.56, 131.09, 128.78, 128.52, 128.48, 128.25, 127.87, 124.18, 123.50, 121.15, 112.46, 70.59. Molecular formula $C_{22}H_{18}O_2$ (HRMS) Calculated = 314.3771, Observed = 314.3797.

### 2.1.6 | (2Z)-3-[2-(benzyloxy)phenyl]-1-(4-chlorophenyl)prop-2-en-1-one (**BB6**)

1H NMR (500 MHz, Chloroform-d) δ 8.02 (d, *J* = 15.8 Hz, 1H), 7.75–7.62 (m, 2H), 7.69 (d, 1H), 7.60–7.58 (m, 1H) 7.51–7.48 (m, 2H), 7.46–7.42 (m, 3H), 7.39–7.33 (m, 3H) 7.05–7.01 (m, 2H), 5.16 (s, 2H); $^{13}$C NMR (126 MHz, $CDCl_3$) δ 189.72, 158.37, 141.50, 138.83, 136.69, 131.74, 131.52, 129.92, 128.81, 128.75, 128.37, 128.03, 123.04, 121.19, 112.40, 70.65. Molecular formula $C_{22}H_{17}O_2Cl$ (HRMS) Calculated = 348.8221, Observed = 348.8197.

### 2.1.7 | (2Z)-3-[2-(benzyloxy) phenyl]-1-(4-bromophenyl) prop-2-en-1-one (**BB7**)

$^1$H NMR (500 MHz, Chloroform-*d*) δ 8.02 (d, *J* = 15.8 Hz, 1H), 7.77–7.62 (m, 3H), 7.59 (dd, *J* = 7.6, 1.8 Hz, 1H), 7.54–7.41 (m, 7H), 7.41–7.34 (m, 1H), 7.02 (ddd, *J* = 8.6, 7.6, 1.8 Hz, 2H), 5.15 (s, 2H). $^{13}$C NMR (126 MHz, $CDCl_3$) δ 189.92, 158.37, 141.57, 137.11, 136.36, 131.74, 131.50, 130.06, 128.82, 128.38, 128.03, 127.54, 123.92, 122.98, 121.20, 121.18, 112.41, 70.65. Molecular formula $C_{22}H_{17}O_2Br$ (HRMS) Calculated = 393.2731, Observed = 393.2697.

#### 2.1.8 | (2Z)-3-[2-(benzyloxy) phenyl]-1-(4-fluorophenyl) prop-2-en-1-one (**BB8**)

$^1$H NMR (500 MHz, Chloroform-*d*) δ 8.02 (d, *J* = 15.8 Hz, 1H), 7.84–7.81 (m, 2H), 7.74–7.71 (dd, 1H), 7.59–7.58 (d, 1H), 7.51–7.49 (m, 2H), 7.45–7.41 (m, 3H),7.37–7.35 (m, 1H), 7.06–7.00 (m, 4H) 5.16 (s, 2H). $^{13}$C NMR (126 MHz, $CDCl_3$) δ 189.34, 166.43, 158.35, 141.18, 136.39, 134.73, 131.64, 131.52, 131.10, 128.80, 128.05, 124.00, 123.15, 121.18, 115.60, 115.43, 112.39, 70.63. Molecular formula $C_{22}H_{17}O_2Br$ (HRMS) Calculated = 332.3676, Observed = 332.3697.

### 2.2 | Enzyme inhibition studies of hMAO-A and hMAO-B

As previously mentioned, MAO-A and MAO-B activities were continuously monitored for 45 min at 316 nm using 0.06 mM of kynuramine and at 250 nm using 0.3 mM of benzylamine, respectively (Mathew et al., 2018). MAO enzymes used were recombinant human MAO-A and MAO-B. Enzymes, substrates, and reference compounds were purchased from Sigma-Aldrich (St. Louis, MO, USA).

#### 2.2.1 | Enzyme inhibition and kinetic studies

The inhibitory activities of MAO-A and MAO-B were initially measured at a concentration of 10 μM inhibitor, and the $IC_{50}$ values for the compound showing a residual activity of less than 50% were then determined by measuring the activity at various concentrations of the compounds and by using GraphPad Prism software 5. The selectivity index (SI) value of MAO-B was calculated by ($IC_{50}$ of MAO-A)/($IC_{50}$ of MAO-B). Kinetic parameters, inhibitor type, and $K_i$ value of the compound for MAO-B were determined by measuring enzyme activity at three different inhibitor concentrations (0.5–2 × $IC_{50}$) and at five different substrate concentrations (0.0375–0.6 mM). The Lineweaver-Burk (LB) plots and their secondary plots were used to compare the enzyme kinetics patterns in order to determine the kind of inhibition (Mathew et al., 2021).

#### 2.2.2 | Reversibility analysis of **BB2** and **BB4**

The reversibility of MAO-B inhibition by **BB2** and **BB4** was evaluated after preincubation for 30 min at ~1.5 × $IC_{50}$, as previously described (Baek et al., 2019). For comparison with lead compounds, lazabemide (a reference reversible MAO-B inhibitor) and pargyline (a reference irreversible MAO-B inhibitor) were preincubated at ~1.5 × $IC_{50}$ (0.15 and 0.10 μM, respectively). Reversibility patterns were analyzed and determined by comparing the activities of dialyzed ($A_D$) and undialyzed ($A_U$) samples (Baek et al., 2019).

### 2.3 | Blood–brain barrier (BBB) permeability study

Parallel artificial membrane permeability assay (PAMPA) method is utilized for the BBB permeation of lead compounds BB2 and BB4. The detailed procedure is deposited in the supporting informations (Di et al., 2003).

### 2.4 | Computational studies

#### 2.4.1 | Target prediction

Target predictions for the lead molecules were done by an online free web-based program (www.swisstargetprediction.ch) (Daina et al., 2019).

#### 2.4.2 | Molecular docking

The three-dimensional X-ray structures of MAO-B (PDB ID: 2V5Z) were first retrieved from the Protein Data Bank (PDB) (Binda et al., 2007). The target structure was improved by the Protein Preparation Wizard (Schrödinger Suite 2021–4) (Schrödinger Release 2021–4: Protein preparation wizard, 2021) in order to correct bond order, add hydrogen atoms and possible missing amino acidic side chains and loops. The 3D conformations of the **BB2** and **BB4** were analyzed by LigPrep (Schrödinger Suite 2021–4) (Schrödinger Release 2021–4: LigPrep, 2021) to generate all possible tautomers and ionization states at pH 7.4, a physiological pH. A cubic grid was automatically generated, centering on the cognate ligand (i.e., safinamide, 12 × 12 × 12 Å and 28 × 28 × 28 Å for the inner and outer boxes, respectively). Docking simulations were carried out using Grid-based Ligand Docking with Energetics (GLIDE) v.9.1 (Friesner et al., 2004; Schrödinger Release 2021–4: Glide, 2021), a part of the Schrödinger Suite 2021–4. Standard precision (SP) was done by the default settings with the Force Field OPLS_2005. The reliability of SP simulation protocol was previously challenged by computing the Root Mean Square Deviations (RMSD) values of the cognate ligands.

#### 2.4.3 | Molecular dynamics (MD)

The MD studies for the lowest docking pose of compound **BB4** were carried out using the Desmond package

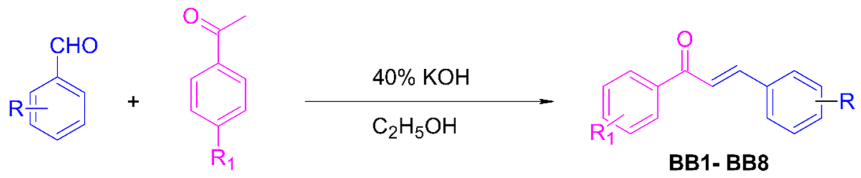


**SCHEME 1** Synthesis of targeted molecules (**BB1**-**BB8**).

| Code | R | $R_1$ | Code | R | $R_1$ |
|---|---|---|---|---|---|
| $BB_1$ | 4-Benzyloxy | H | $BB_5$ | 2-Benzyloxy | H |
| $BB_2$ | 4-Benzyloxy | Cl | $BB_6$ | 2-Benzyloxy | Cl |
| $BB_3$ | 4-Benzyloxy | F | $BB_7$ | 2-Benzyloxy | F |
| $BB_4$ | 4-Benzyloxy | Br | $BB_8$ | 2-Benzyloxy | Br |

(Desmond V 7.2), which was installed on a Dell Inc. Precision 7820 Tower with the configuration Ubuntu 22.04.1 LTS 64-bit, Intel Xenon (R) silver 4210R, and NVIDIA Corporation GP104GL (RTX A 4000) graphics processing unit (Desmond Molecular Dynamics System, 2021). Detailed MD investigation conditions such as solvent simulation box shape, size, barometer and thermostat parameters, long and short-range interaction calculations were described previously (Koyiparambath et al., 2021; Mathew et al., 2016). To evaluate the domain correlations, RMSD, RMSF, and protein ligand contact across all C atoms were analyzed during the 100 ns MD simulation. Then, the MD trajectory for examining the dynamics of protein-ligand interaction was selected at 100 ps intervals with 1000 frames generated for each.

## 3 | RESULTS AND DISCUSSION

### 3.1 | Chemistry

Scheme 1 shows the synthesis of the titled candidates and the spectra are provided in Appendix Appendix S1. The existence of the methylene group in the benzyloxy portion was verified by a sharp singlet of 5.11–5.17 in the $^1$H–NMR spectrum. A significant coupling constant of the double bond of 15 Hz indicated that the chalcone was in a *trans* configuration. Information on the conformation of the carbonyl carbon's $sp^2$ nature in the linker of chalcones was supplied by the carbonyl carbon at 188.88–191.05 in the $^{13}$C-NMR spectra. The molecular weights of the targeted substances were identified by the HRMS analysis. The calculated molecular weight of the compounds is in accordance with the observed value. Among halogen atoms, iodine atom is less attractive in chemical synthesis due to its stability (i.e., photoreactive) and cost, and it was not included in this study.

### 3.2 | Enzyme inhibition assay

#### 3.2.1 | Inhibition studies of MAO-A and MAO-B

Eight chalcone derivatives were synthesized, and their ability to inhibit MAO-A and MAO-B was examined. All compounds had more potent MAO-B inhibitory action than MAO-A. MAO-B inhibitory activity was tested at 1.0 μM, since the preliminary results revealed that the *para*-$C_6H_5H_2CO$ substituted derivatives had extremely low residual activities of <50% for MAO-B at a concentration of 10 μM (Table 1). Compound **BB4** most potently inhibited MAO-B with an $IC_{50}$ value of 0.062 μM, followed by **BB2** ($IC_{50}$ = 0.093 μM). Structurally, *para*-$C_6H_5H_2CO$ substituted derivatives (**BB1**-**BB4**) in the **B**-ring showed higher MAO-B inhibitory activities than the *ortho*-$C_6H_5H_2CO$ substituted derivatives (**BB5**-**BB8**). In addition, in *para*-$C_6H_5H_2CO$ substituted derivatives, the -Br (**BB4**) substitution at the *para* position of the **A**-ring showed the highest MAO-B inhibition, followed by -Cl (**BB2**) substitution. MAO-B inhibition of -Br substituent (**BB4)** was 4.16 times higher than -H (**BB1**, basic structure) and 1.5 times higher than -Cl (**BB2**). Potencies for MAO-B inhibitory activity as follow: -Br (**BB4**) > -Cl (**BB2**) > -H (**BB1**) > -F (**BB3**). Selectivity index (SI) values for MAO-B of **BB2** and **BB4** were calculated as 430.108 and 645.161, respectively. However, all derivatives showed weak inhibitory activity against MAO-A. These results suggested that **BB2** and **BB4** were potent selective MAO-B inhibitors.

**TABLE 1** Inhibitions of MAO-A and MAO-B by **BB** series.[a]

| | Residual activity (%) | | $IC_{50}$ (μM) | | |
|---|---|---|---|---|---|
| | MAO-A | MAO-B | | | |
| **Compound** | **10 μM** | **1 μM** | **MAO-A** | **MAO-B** | **SI[b]** |
| **BB1** | 79.92 ± 1.52 | 11.96 ± 0.63 | >40 | 0.258 ± 0.001 | >155.039 |
| **BB2** | 90.23 ± 2.50 | 11.96 ± 0.63 | >40 | 0.093 ± 0.009 | >430.108 |
| **BB3** | 91.21 ± 2.53 | 33.69 ± 1.19 | >40 | 0.583 ± 0.068 | >68.611 |
| **BB4** | 98.54 ± 0.65 | 15.95 ± 2.21 | >40 | 0.062 ± 0.012 | >645.161 |
| **BB5** | 87.50 ± 0.71 | 88.02 ± 2.27 | >40 | 26.642 ± 0.614 | >1.501 |
| **BB6** | 89.50 ± 0.71 | 78.46 ± 1.11 | >40 | 9.401 ± 0.245 | >4.255 |
| **BB7** | 89.50 ± 2.12 | 97.55 ± 6.14 | >40 | 17.360 ± 0.618 | >2.304 |
| **BB8** | 97.50 ± 0.71 | 99.49 ± 3.39 | >40 | 6.927 ± 2.325 | >5.775 |
| Toloxatone | | | 1.080 ± 0.025 | – | |
| Lazabemide | | | – | 0.110 ± 0.016 | |
| Clorgyline | | | 0.007 ± 0.001 | – | |
| Pargyline | | | – | 0.140 ± 0.006 | |

[a]Selectivity index (SI) values are expressed for MAO-B as compared with MAO-A.

[b]Results are the means ± standard errors of duplicate or triplicate experiments.

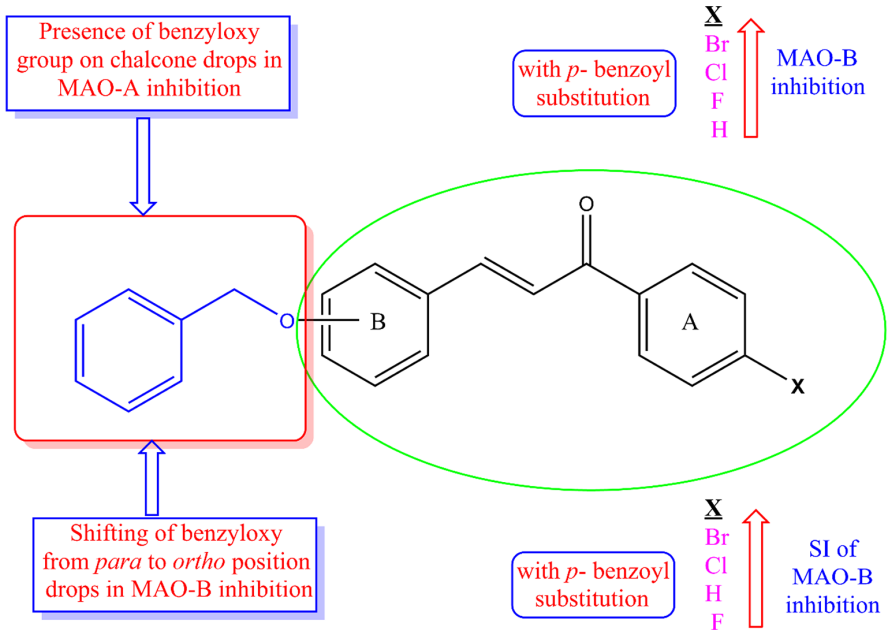


**FIGURE 2** SAR pattern of benzyloxy-derived halogenated chalcones.

Based on the orientation pattern of the benzyloxy groups on the various locations of the phenyl ring **B** and the presence of various halogens on the *para*-position of chalcones ring **A**, it is feasible to construct variety of significant structure–activity relationships (SARs). The outcomes unmistakably showed that all of the halogenated chalcone derivatives synthesized from *para*-substituted benzyloxy inhibited MAO-B in a good to outstanding manner. Given the orientation pattern, it is clear that the insertion of benzyloxy groups at the 2′ position on the **B** ring of the chalcone framework has less inhibitory activities than the 4′ positions. In terms of MAO-B inhibitory effectiveness, bromine or chlorine substituted on the **A** ring performed better than fluorine substituted on it. It is interesting to note that the reference drugs lazabemide and pargyline are both outperformed by the most potent molecule, **BB4**, by 1.7 and 2.25 times, respectively. A visual illustration of SARs is shown in Figure 2.

Recent studies documented that presence of electron donating groups on the *para* position of ring **B** of chalcone framework showed significant MAO-B inhibition. Shifting of benzyloxy pharmacophore from *ortho* to *para* position may accommodate more steric hindrance, nearer to the α, β-unsaturated system. This would probably make

less binding interactions in the active MAO-B site (Kumar et al., 2023; Sudevan, Oh, et al., 2022).

### 3.2.2 | Kinetic studies

Modes of MAO-B inhibition by **BB2** and **BB4** were investigated using Lineweaver-Burk plots. Plots of MAO-B inhibition by **BB2** and **BB4** were linear and the lines seemed to be intersected at Y-axis and showed that **BB2** and **BB4** were competitive inhibitors of MAO-B (Figure 3a,c). Secondary plots of the slopes of Lineweaver–Burk plots against inhibitor concentrations showed that the $K_i$ values of **BB2** and **BB4** were $0.030 \pm 0.014$ and $0.011 \pm 0.005\,\mu M$, respectively (Figure 3b,d). These results suggested that **BB2** and **BB4** were competitive inhibitors of MAO-B.

### 3.2.3 | Reversibility

After preincubating MAO-B with **BB2** or **BB4** for 30 min, the reversibility study of the inhibitors was examined using dialysis. The following concentrations were used in the experiments: **BB2** and **BB4** at 0.15 and 0.10 μM, respectively; lazabemide (a reference reversible inhibitor) at 0.22 μM; and pargyline (a reference irreversible inhibitor) at 0.28 μM. To identify the reversibility patterns, the relative activities of samples that had been dialyzed ($A_D$) and those that had not been dialyzed ($A_U$) were compared. The inhibition of MAO-B by **BB2** and **BB4** recovered from 36.0% ($A_U$) to 88.5% ($A_D$) and 43.0% ($A_U$) to 91.5% ($A_D$), respectively, in reversibility assays employing dialysis (Figure 4). These sample recovery rates were similar to those for lazabemide ranged from 28.3% to 86.2%, but not to those for pargyline ranged from 33.3% to 40.8%, indicating that **BB2** and **BB4** were reversible MAO-B inhibitors.

## 3.3 | BBB permeation study

PAMPA manifested that the halogenated benzyloxy chalcones (**BB2** and **BB4**) had a significant permeability and CNS bioavailability with *Pe* value higher than $4.0 \times 10^{-6}$ cm/s (Table 2). The results documented that the lead molecules exhibited good BBB permeation and suitable for CNS targeted drug delivery.

## 3.4 | Computational investigation

### 3.4.1 | Swiss target prediction

Previously the basic framework of chalcone is predicted as a prominent target for MAOs, especially MAO-B. In the current study, the lead molecules **BB2** and **BB4** gave the highest probability in a target class of

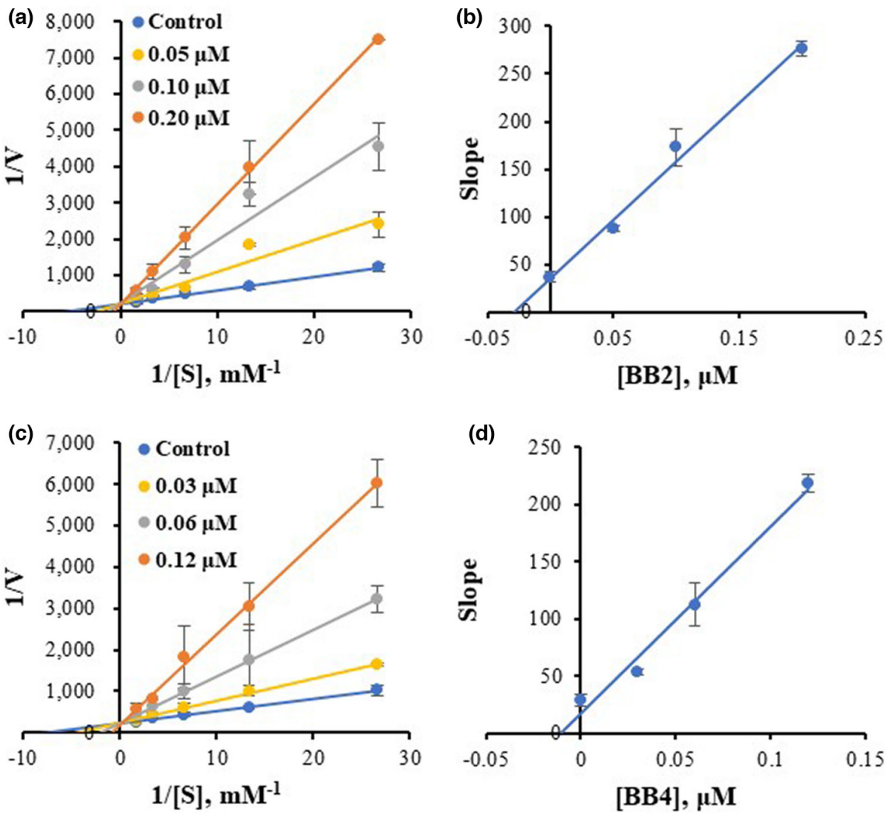


FIGURE 3 Lineweaver–Burk plots for MAO-B inhibition by **BB2** and **BB4** (a, c), and their respective secondary plots (b, d) of the slopes vs. inhibitor concentrations.

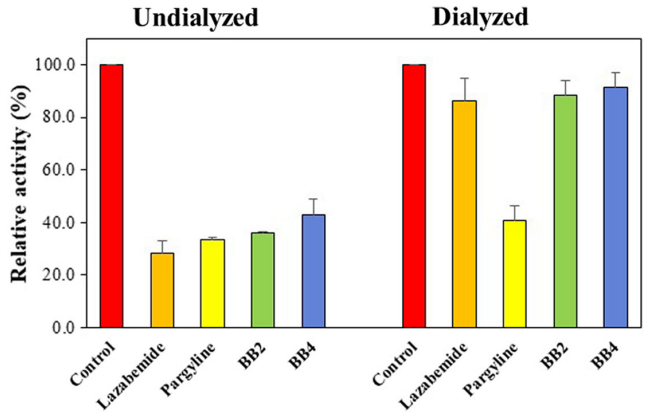


**FIGURE 4** Recoveries of MAO-B inhibitions by **BB2** and **BB4** using dialysis experiments.

**TABLE 2** Blood–Brain Barrier assay of key compounds of halogenated benzyloxy chalcones by PAMPA method.

| Compounds | Experimental *Pe* ($\times 10^{-6}$ cm/s) | Prediction |
|---|---|---|
| BB2 | 4.04 ± 0.21 | CNS+ |
| BB4 | 5.03 ± 0.14 | CNS+ |
| Selegiline | 5.69 ± 0.04 | CNS+ |

*Note*: *Pe* ($10^{-6}$ cm/s) > 4.00: CNS+ (high permeation); *Pe* ($10^{-6}$ cm/s) < 2.00: CNS− (low permeation); *Pe* ($10^{-6}$ cm/s) from 2.00 to 4.00: CNS ± (BBB permeation uncertain).

oxidoreductase with MAO-B (Figure 5). Both structures consist of (2*E*)-1,3-diphenylprop-2-en-1-one (chalcone), with the presence of halogens on the **A** ring and benzyloxy pharmacophore on the *para* position of **B** ring. All these structural features are the important pharmacophore requirements for the development MAO-B inhibitors.

### 3.4.2 | Molecular docking studies

Glide SP docking was used to analyze the molecular basis of the interaction and conformation of **BB4** and **BB2** in the target protein MAO-active B's site, and docking simulations were utilized to examine how **BB2** and **BB4** bind to the crystal structure of MAO-B (Figure 6). Figure 7 shows the key binding residues of both drugs against MAO-B.

Overall, the molecular docking analyses of both compounds provided a sound rationale for the observed bioactivities. The $IC_{50}$ values were correlated well with the docking scores equal to −8.600 and −8.233 kcal/mol for **BB4** and **BB2**, respectively. The main molecular interactions are depicted in Figure 7. The **BB2** and **BB4** majorly interacted with Y326 through π−π stacking. The docking score of native ligand (safinamide) was found to be −9.10 kcal/mol.

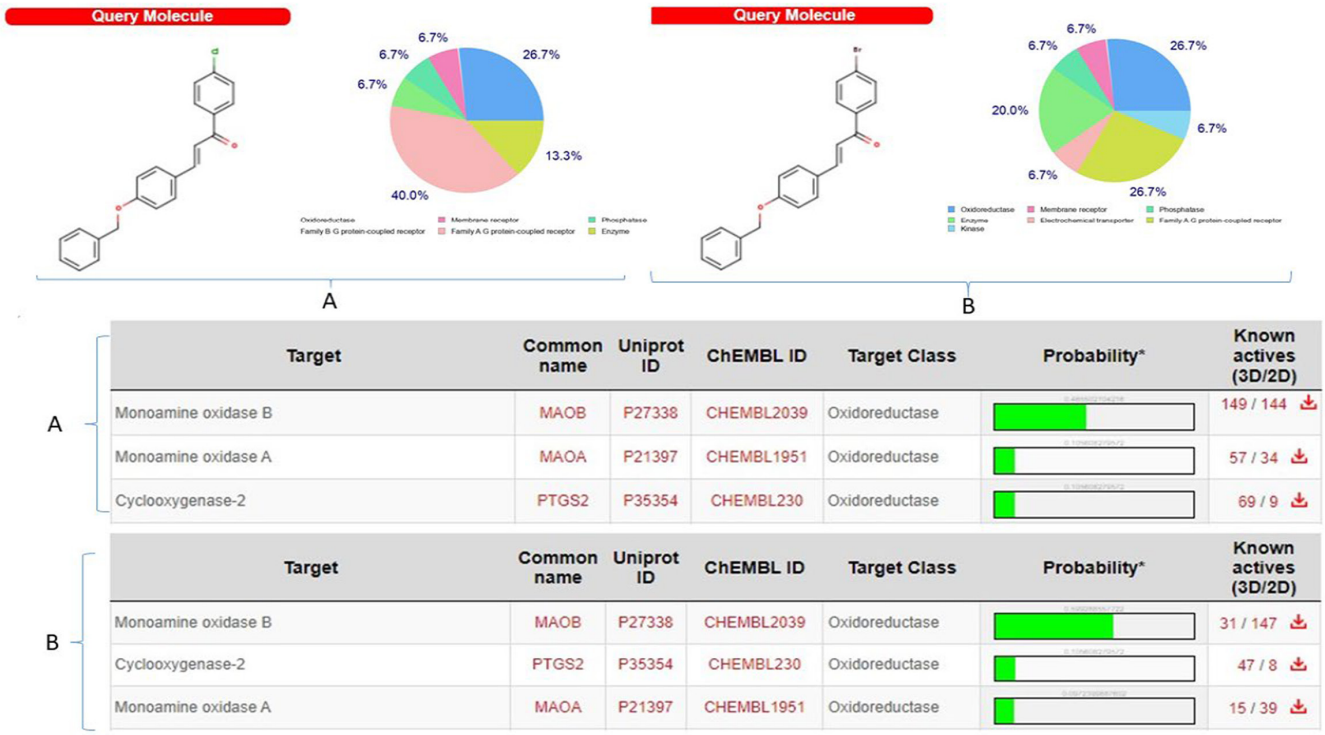


A

| Target | Common name | Uniprot ID | ChEMBL ID | Target Class | Probability* | Known actives (3D/2D) |
|---|---|---|---|---|---|---|
| Monoamine oxidase B | MAOB | P27338 | CHEMBL2039 | Oxidoreductase | | 149 / 144 |
| Monoamine oxidase A | MAOA | P21397 | CHEMBL1951 | Oxidoreductase | | 57 / 34 |
| Cyclooxygenase-2 | PTGS2 | P35354 | CHEMBL230 | Oxidoreductase | | 69 / 9 |

B

| Target | Common name | Uniprot ID | ChEMBL ID | Target Class | Probability* | Known actives (3D/2D) |
|---|---|---|---|---|---|---|
| Monoamine oxidase B | MAOB | P27338 | CHEMBL2039 | Oxidoreductase | | 31 / 147 |
| Cyclooxygenase-2 | PTGS2 | P35354 | CHEMBL230 | Oxidoreductase | | 47 / 8 |
| Monoamine oxidase A | MAOA | P21397 | CHEMBL1951 | Oxidoreductase | | 15 / 39 |

**FIGURE 5** Target prediction of **BB2** (A) and **BB4** (B).

### 3.4.3 | Molecular dynamics

The MD simulation is utilized in drug discovery research to reproduce the nearly precise or realistic dynamic behavior of a protein–ligand complex while providing time-affordable comprehension of energetic information regarding protein and ligand interactions. This study used MD modelling in biological contexts to model **BB4** at the MAO-B protein's binding site. Using the MD trajectories, the root-mean-square deviation (RMSD), root-mean-square fluctuation (RMSF), and protein–ligand interactions were computed.

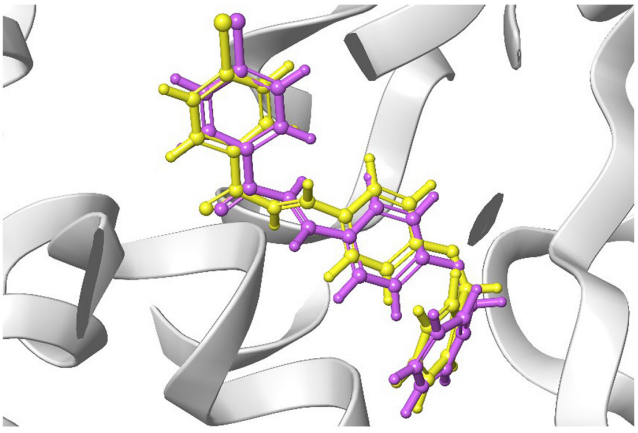

**FIGURE 6** Overlap of docking poses of **BB4** and **BB2** rendering in pink and yellow ball-sticks, respectively.

Several MD trajectory data analyses for the **BB4**-MAO-B complex are shown in Figure 8(a–d). Protein–ligand complex were simulated using water molecules. The RMSD in Figure 8a showed a stable protein–ligand combination over the simulation period, with RMSD values for protein C atoms in the complex with ligand ranging from 0.92 to 2.44. For the compound **BB4** RMSD with reference to protein, the ligand RMSD ranged from 2.0 to 3.52. With the exception of a little change, the simulation's RMSD for **BB4** was found to be constant. The greatest ligand RMSD values of 3.49 and 3.52 were observed at 13 and 46 ns, respectively. The RMSD plot's overall result demonstrated that the ligand was stable with regard to the protein and its binding site. By determining the RMSF of each individual protein amino acid residue, the flexibility of the protein system was also evaluated during the simulation. The RMSF plot (Figure 8b) clearly showed that the 333–336 amino acids as well as the N- and C-terminal residues had relatively few fluctuations and the majority of higher fluctuations. The following amino acids had significant interactions with the ligand: Pro104 (0.89), Tyr326

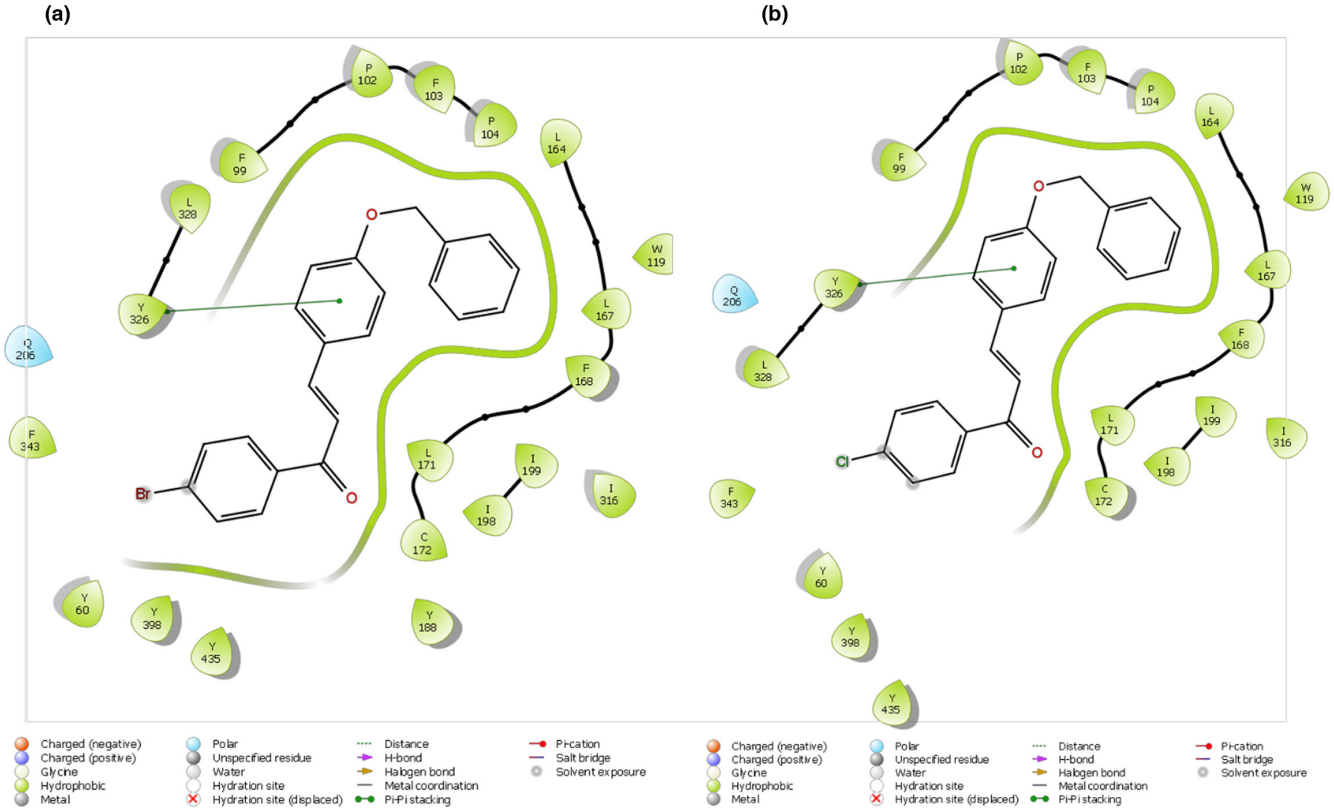


**FIGURE 7** 2D interactions of **BB4** (a) and **BB2** (b) toward MAO-B (PDB entry: 2V5Z).

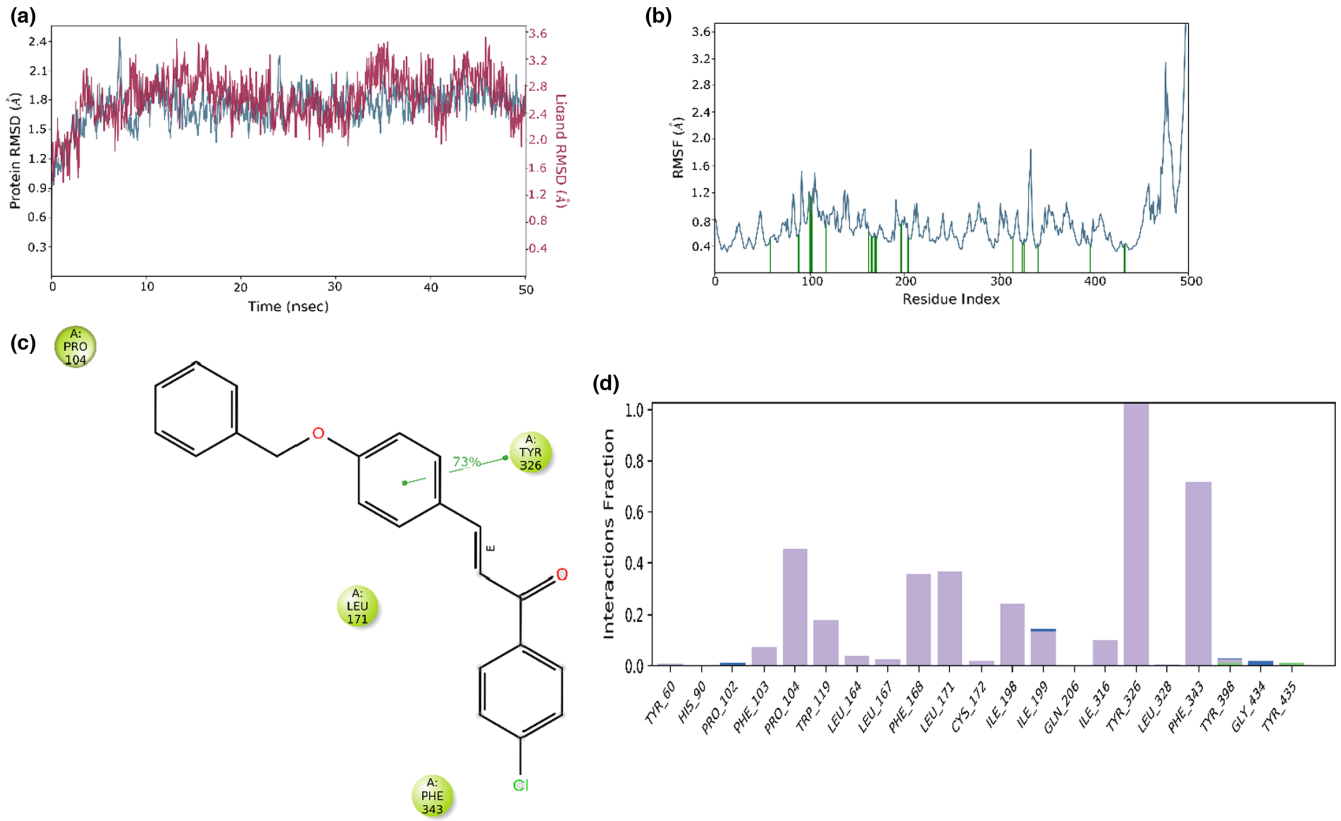


**FIGURE 8** Analysis of the **BB4**-MAO-B complex using MD simulation. (a) RMSD (blue, MAO-B; red, **BB4**-MAO-B complex). (b) Individual amino acid RMSF for proteins. (c) 2-D Interaction diagram. (d) Analysis of the MD trajectory's protein–ligand contacts.

(0.43), Leu171 (0.57), and Phe343 (0.41). All of these interacting residues had RMSF values between 0.41 and 0.89. Majority hydrophobic contact occurred in protein–ligand interaction. Figure 8c and d demonstrated how hydrophobic stability was provided by the ligand–protein complex. Tyr326 participated in 73% of the simulation time in 2D interaction with π−π stacking. In MD simulations, the physiological environment was more accurately mirrored for better understanding binding patterns. The trajectory analysis and overall MD simulation indicated that the hit molecule could inhibit MAO-B.

## 4 | CONCLUSION

The present study aimed to incorporate the benzyloxy pharmacophore to the *ortho* and *para* positions of ring **B** and to evaluate the influence of halogens on the *para* position of phenyl **B** ring of chalcone framework toward MAO inhibition. Contrary to *ortho*-$C_6H_5H_2CO$ substituted derivatives (**BB5-BB8**), *para*-substituted $C_6H_5H_2CO$ compounds (**BB1-BB4**) on the **B**-ring showed stronger MAO-B inhibitory activity. The **A**-ring substitution with -Br (**BB4**) and -Cl (**BB2**) demonstrated the strongest MAO-B inhibition in the derivatives substituted with *para*-$C_6H_5H_2CO$. The reversibility and kinetics tests claimed that lead molecules **BB2** and **BB4** showed reversible and competitive mode of inhibition. In docking studies, we observed that both lead compounds attached to MAO-B with consistent origin and docking scores. The Phe326 (73%) with π−π stacking was found to give stability in the complex in MD simulation studies. These lead structures can be taken into consideration for the new class of MAO-B inhibitors for the treatment of neuro-related illnesses due to their higher potency than the reference MAO-B inhibitors.

## ACKNOWLEDGEMENTS

None.

## DATA AVAILABILITY STATEMENT

The data that supports the findings of this study are available in the supplementary material of this article.

## ORCID

*Orazio Nicolotti* https://orcid.org/0000-0001-6533-5539

## REFERENCES

Abell, C. W., & Kwan, S. W. (2001). Molecular characterization of monoamine oxidases A and B. *Progress in Nucleic Acid Research*

*and Molecular Biology*, *65*, 129–156. https://doi.org/10.1016/s0079-6603(00)65004-3a

Al-Salahi, R., Detlef, G., & Ahmed, B. (2011). 2-Benzyloxy-1,2,4-Triazolo[1,5-*a*]Quinazolin-5(4 *H*)-One. *Acta Crystallographica Section E Structure Reports Online*, *67*, o1861. https://doi.org/10.1107/S1600536811024962

Annapurna, A., Mudagal, M. P., Ansari, A., & Rao, A.S. (2012). Cardioprotective activity of chalcones in ischemia/reperfusion-induced myocardial infarction in albino rats. *Experimental Clinical Cardiology*, *17*, 110–114.

Baek, S. C., Park, M. H., Ryu, H. W., Lee, J. P., Kang, M.-G., Park, D., Park, C. M., Oh, S.-R., & Kim, H. (2019). Rhamnocitrin isolated from prunus Padus var. Seoulensis: A potent and selective reversible inhibitor of human monoamine oxidase a. *Bioorganic Chemistry*, *83*, 317–325. https://doi.org/10.1016/j.bioorg.2018.10.051

Binda, C., Wang, J., Pisani, L., Caccia, C., Carotti, A., Salvati, P., Edmondson, D. E., & Mattevi, A. (2007). Structures of human monoamine oxidase B complexes with selective noncovalent inhibitors: Safinamide and coumarin analogs. *Journal of Medicinal Chemistry*, *50*, 5848–5852. https://doi.org/10.1021/jm070677y

Bolasco, A., Carradori, S., & Fioravanti, R. (2010). Focusing on new monoamine oxidase inhibitors. *Expert Opinion on Therapeutic Patents*, *20*, 909–939. https://doi.org/10.1517/13543776.2010.495716

Carradori, S., & Silvestri, R. (2015). New Frontiers in selective human MAO-B inhibitors. *Journal of Medicinal Chemistry*, *58*, 6717–6732. https://doi.org/10.1021/jm501690r

Cheng, P., Yang, L., Huang, X., Wang, X., & Gong, M. (2020). Chalcone hybrids and their antimalarial activity. *Arch Pharm (Weinheim)*, *353*, 1900350. https://doi.org/10.1002/ardp.201900350

Chimenti, F., Secci, D., Bolasco, A., Chimenti, P., Bizzarri, B., Granese, A., Carradori, S., Yáñez, M., Orallo, F., Ortuso, F., & Alcaro, S. (2009). Synthesis, molecular modeling, and selective inhibitory activity against human monoamine oxidases of 3-Carboxamido-7-substituted coumarins. *Journal of Medicinal Chemistry*, *52*, 1935–1942. https://doi.org/10.1021/jm801496u

Daina, A., Michielin, O., & Zoete, V. (2019). SwissTargetPrediction: Updated data and new features for efficient prediction of protein targets of small molecules. *Nucleic Acids Research*, *47*(W1), W357–W364. https://doi.org/10.1093/nar/gkz382

de Lau, L. M., & Breteler, M. M. (2006). Epidemiology of Parkinson's disease. *The Lancet Neurology*, *5*, 525–535. https://doi.org/10.1016/S1474-4422(06)70471-9

de Souza, P. S., Bibá, G. C. C., Melo, E. D. N., & Muzitano, M. F. (2021). Chalcones against the hallmarks of cancer: A mini-review. *Natural Product Research*, *36*, 1–18. https://doi.org/10.1080/14786419.2021.2000980

Desmond Molecular Dynamics System. (2021). D. E. Shaw Research, New York, NY, 2021. Maestro-Desmond interoperability tools, Schrödinger, New York, NY.

Di, L., Kerns, E. H., Fan, K., McConnell, O. J., & Carter, G. T. (2003). High throughput artificial membrane permeability assay for blood-brain barrier. *European Journal of Medicinal Chemistry*, *38*, 223–232.

Edmondson, D. (2004). The FAD binding sites of human monoamine oxidases A and B. *Neurotoxicology*, *25*, 63–72. https://doi.org/10.1016/S0161-813X(03)00114-1

Elkhalifa, D., Al-Hashimi, I., Al Moustafa, A.-E., & Khalil, A. (2021). A comprehensive review on the antiviral activities of chalcones. *Journal of Drug Targeting*, *29*, 403–419. https://doi.org/10.1080/1061186X.2020.1853759

Elmer, L. W., & Bertoni, J. M. (2008). The increasing role of monoamine oxidase type B inhibitors in Parkinson's disease therapy. *Expert Opinion on Pharmacotherapy*, *9*, 2759–2772. https://doi.org/10.1517/14656566.9.16.2759

Fabbrini, G., Abbruzzese, G., Marconi, S., & Zappia, M. (2012). Selegiline. *Clinical Neuropharmacology*, *35*, 134–140. https://doi.org/10.1097/WNF.0b013e318255838b

Fang, W.-Y., Ravindar, L., Rakesh, K. P., Manukumar, H. M., Shantharam, C. S., Alharbi, N. S., & Qin, H.-L. (2019). Synthetic approaches and pharmaceutical applications of Chloro-containing molecules for drug discovery: A critical review. *European Journal of Medicinal Chemistry*, *173*, 117–153. https://doi.org/10.1016/j.ejmech.2019.03.063

Finberg, J. P. M., & Rabey, J. M. (2016). Inhibitors of MAO-A and MAO-B in psychiatry and neurology. *Frontiers in Pharmacology*, *7*, 340. https://doi.org/10.3389/fphar.2016.00340

Friesner, R. A., Banks, J. L., Murphy, R. B., Halgren, T. A., Klicic, J. J., Mainz, D. T., Repasky, M. P., Knoll, E. H., Shelley, M., Perry, J. K., Shaw, D. E., Francis, P., & Shenkin, P. S. (2004). Glide: A new approach for rapid, accurate docking and scoring. 1. Method and assessment of docking accuracy. *Journal of Medicinal Chemistry*, *47*, 1739–1749. https://doi.org/10.1021/jm0306430

Guglielmi, P., Mathew, B., Secci, D., & Carradori, S. (2020). Chalcones: Unearthing their therapeutic possibility as monoamine oxidase B inhibitors. *European Journal of Medicinal Chemistry*, *205*, 112650. https://doi.org/10.1016/j.ejmech.2020.112650

Joy, M., Mathew, B., & Sudarsanakumar, C. (2018). Structural features of safinamide: A combined Hirshfeld surface analysis & quantum chemical treatment. *Chemical Data Collections*, *17–18*, 404–414. https://doi.org/10.1016/j.cdc.2018.10.009

Knez, D., Hrast, M., Frlan, R., Pišlar, A., Žakelj, S., Kos, J., & Gobec, S. (2022). Indoles and 1-(3-(benzyloxy)benzyl)piperazines: Reversible and selective monoamine oxidase B inhibitors identified by screening an in-house compound library. *Bioorganic Chemistry*, *119*, 105581. https://doi.org/10.1016/j.bioorg.2021.105581

Kontogiorgis, C., Mantzanidou, M., & Hadjipavlou-Litina, D. (2008). Chalcones and their potential role in inflammation. *Mini-Reviews in Medicinal Chemistry*, *8*, 1224–1242. https://doi.org/10.2174/138955708786141034

Koyiparambath, V. P., Oh, J. M., Khames, A., Abdelgawad, M. A., Nair, A. S., Nath, L. R., Gambacorta, N., Ciriaco, F., Nicolotti, O., Kim, H., & Mathew, B. (2021). Trimethoxylated halogenated chalcones as dual inhibitors of MAO-B and BACE-1 for the treatment of neurodegenerative disorders. *Pharmaceutics*, *13*, 850. https://doi.org/10.3390/pharmaceutics13060850

Kumar, S., Nair, A. S., Bhashkar, V., Sudevan, S. T., Koyiparambath, V. P., Khames, A., Abdelgawad, M. A., & Mathew, B. (2021). Navigating into the chemical space of monoamine oxidase inhibitors by artificial intelligence and cheminformatics approach. *ACS Omega*, *6*, 23399–23411. https://doi.org/10.1021/acsomega.1c03250

Kumar, S., Oh, J. M., Abdelgawad, M. A., Abourehab, M. A. S., Tengli, A. K., Singh, A. K., Ahmad, I., Patel, H., Mathew, B., &

Kim, H. (2023). Development of isopropyl-tailed chalcones as a new class of selective MAO-B inhibitors for the treatment of Parkinson's disorder. *ACS. Omega*, *8*(7), 6908–6917. https://doi.org/10.1021/acsomega.2c07694

Mathew, B., Baek, S. C., Grace Thomas Parambi, D., Pil Lee, J., Joy, M., Annie Rilda, P. R., Randev, R. V., Nithyamol, P., Vijayan, V., Inasu, S. T., et al. (2018). Selected aryl thiosemicarbazones as a new class of multi-targeted monoamine oxidase inhibitors. *Medchemcomm*, *9*, 1871–1881. https://doi.org/10.1039/c8md00399h

Mathew, B., Carradori, S., Guglielmi, P., Uddin, M. S., & Kim, H. (2020). New aspects of monoamine oxidase B inhibitors: The key role of halogens to open the Golden door. *Current Medicinal Chemistry*, *28*, 266–283. https://doi.org/10.2174/0929867327666200121165931

Mathew, B., Haridas, A., Uçar, G., Baysal, I., Joy, M., Mathew, G. E., Lakshmanan, B., & Jayaprakash, V. (2016). Synthesis, biochemistry, and computational studies of brominated thienyl chalcones: A new class of reversible MAO-B inhibitors. *ChemMedChem*, *11*, 1161–1171.

Mathew, B., Mathew, G. E., Uçar, G., Baysal, I., Suresh, J., Vilapurathu, J. K., Prakasan, A., Suresh, J. K., & Thomas, A. (2015). Development of fluorinated methoxylated chalcones as selective monoamine oxidase-B inhibitors: Synthesis, biochemistry and molecular docking studies. *Bioorganic Chemistry*, *62*, 22–29. https://doi.org/10.1016/j.bioorg.2015.07.001

Mathew, B., Oh, J. M., Abdelgawad, M. A., Khames, A., Ghoneim, M. M., Kumar, S., Nath, L. R., Sudevan, S. T., Parambi, D. G. T., Agoni, C., Soliman, M. E. S., & Kim, H. (2022). Conjugated Dienones from differently substituted cinnamaldehyde as highly potent monoamine oxidase-B inhibitors: Synthesis, biochemistry, and computational chemistry. *ACS Omega*, *7*, 8184–8197. https://doi.org/10.1021/acsomega.2c00397

Mathew, B., Oh, J. M., Baty, R. S., Batiha, G. E.-S., Parambi, D. G. T., Gambacorta, N., Nicolotti, O., & Kim, H. (2021). Piperazine-substituted chalcones: A new class of MAO-B, AChE, and BACE-1 inhibitors for the treatment of neurological disorders. *Environmental Science and Pollution Research International*, *28*, 38855–38866. https://doi.org/10.1007/s11356-021-13320-y

Mathew, B., Parambi, D. G. T., Sivasankarapillai, V. S., Uddin, M. S., Suresh, J., Mathew, G. E., Joy, M., Marathakam, A., & Gupta, S. V. (2019). Perspective Design of Chalcones for the management of CNS disorders: A mini-review. *CNS & Neurological Disorders Drug Targets*, *18*, 432–445. https://doi.org/10.2174/1871527318666190610111246

Mellado, M., Salas, C. O., Uriarte, E., Viña, D., Jara-Gutiérrez, C., Matos, M. J., & Cuellar, M. (2019). Design, synthesis and docking calculations of prenylated chalcones as selective monoamine oxidase B inhibitors with antioxidant activity. *ChemistrySelect*, *4*, 7698–7703. https://doi.org/10.1002/slct.201901282

Mostert, S., Petzer, A., & Petzer, J. P. (2017). The evaluation of 1,4-benzoquinones as inhibitors of human monoamine oxidase. *European Journal of Medicinal Chemistry*, *135*, 196–203. https://doi.org/10.1016/j.ejmech.2017.04.055

Parambi, D. G. T., Oh, J. M., Baek, S. C., Lee, J. P., Tondo, A. R., Nicolotti, O., Kim, H., & Mathew, B. (2019). Design, synthesis and biological evaluation of oxygenated chalcones as potent and selective MAO-B inhibitors. *Bioorganic Chemistry*, *93*, 103335. https://doi.org/10.1016/j.bioorg.2019.103335

Pérez, V., Marco, J. L., Fernández-Álvarez, E., & Unzeta, M. (1999). Relevance of benzyloxy group in 2-indolyl methylamines in the selective MAO-B inhibition. *British Journal of Pharmacology*, *127*, 869–876. https://doi.org/10.1038/sj.bjp.0702600

Rao, Y. J., Abhijit, K., Mallikarjun, G., & Hemasri, Y. (2021). Design and synthesis of novel benzyloxy-tethered-chromone-carboxamide derivatives as potent and selective human monoamine oxidase-b inhibitors. *Chemical Papers*, *75*, 703–716. https://doi.org/10.1007/s11696-020-01332-w

Robakis, D., & Fahn, S. (2015). Defining the role of the monoamine oxidase-B inhibitors for Parkinson's disease. *CNS Drugs*, *29*, 433–441. https://doi.org/10.1007/s40263-015-0249-8

Rullo, M., Catto, M., Carrieri, A., de Candia, M., Altomare, C. D., & Pisani, L. (2019). Chasing ChEs-MAO B multi-targeting 4-Aminomethyl-7-benzyloxy-2H-Chromen-2-ones. *Molecules*, *24*, 4507. https://doi.org/10.3390/molecules24244507

Schapira, A. H. V. (2011). Monoamine oxidase B inhibitors for the treatment of Parkinson's disease. *CNS Drugs*, *25*, 1061–1071.

Schrödinger Release 2021–4: Glide. (2021). Schrödinger, LLC, New York, NY.

Schrödinger release 2021–4: LigPrep. (2021). Schrödinger, LLC, New York, NY.

Schrödinger Release 2021–4: Protein preparation wizard. (2021). Epik, Schrödinger, LLC, New York, NY, 2021; Impact, Schrödinger, LLC, New York, NY; Prime, Schrödinger, LLC, New York, NY, 2021.

Shih, J. C., & Chen, K. (2004). Regulation of MAO-A and MAO-B gene expression. *Current Medicinal Chemistry*, *11*, 1995–2005. https://doi.org/10.2174/0929867043364757

Sousa, A., Ribeiro, D., Fernandes, E., & Freitas, M. (2021). The effect of chalcones on the Main sources of reactive species production: Possible therapeutic implications in diabetes mellitus. *Current Medicinal Chemistry*, *28*, 1625–1669. https://doi.org/10.2174/0929867327666200525010007

Sudevan, S. T., Oh, J. M., Abdelgawad, M. A., Abourehab, M. A. S., Rangarajan, T. M., Kumar, S., Ahmad, I., Patel, H., Kim, H., & Mathew, B. (2022). Introduction of benzyloxy pharmacophore into aryl/heteroaryl chalcone motifs as a new class of monoamine oxidase B inhibitors. *Scientific Reports*, *12*(1), 22404. https://doi.org/10.1038/s41598-022-26929-x

Sudevan, S. T., Rangarajan, T. M., Al-Sehemi, A. G., Nair, A. S., Koyiparambath, V. P., & Mathew, B. (2022). Revealing the role of the benzyloxy pharmacophore in the Design of a new Class of monoamine oxidase-B inhibitors. *Arch Pharm (Weinheim)*, *355*, e2200084. https://doi.org/10.1002/ardp.202200084

Tan, Y. Y., Jenner, P., & Chen, S. D. (2022). Monoamine oxidase-B inhibitors for the treatment of Parkinson's disease: Past, present, and *future*. *Journal of Parkinson's Disease*, *12*, 477–493.

Tripathi, R. K. P., & Ayyannan, S. R. (2019). Monoamine oxidase-B inhibitors as potential neurotherapeutic agents: An overview and update. *Medicinal Research Reviews*, *39*, 1603–1706. https://doi.org/10.1002/med.21561

Xu, M., Wu, P., Shen, F., Ji, J., & Rakesh, K. P. (2019). Chalcone derivatives and their antibacterial activities: Current development. *Bioorganic Chemistry*, *91*, 103133. https://doi.org/10.1016/j.bioorg.2019.103133

Zhuang, C., Zhang, W., Sheng, C., Zhang, W., Xing, C., & Miao, Z. (2017). Chalcone: A privileged structure in medicinal chemistry. *Chemical Reviews*, *117*, 7762–7810. https://doi.org/10.1021/acs.chemrev.7b00020

## SUPPORTING INFORMATION

Additional supporting information can be found online in the Supporting Information section at the end of this article.

**How to cite this article:** Singh, A. K., Kim, S.-M., Oh, J. M., Abdelgawad, M. A., Ghoneim, M. M., Rangarajan, T. M., Kumar, S., Sudevan, S. T., Trisciuzzi, D., Nicolotti, O., Kim, H., & Mathew, B. (2023). Exploration of a new class of monoamine oxidase B inhibitors by assembling benzyloxy pharmacophore on halogenated chalcones. *Chemical Biology & Drug Design*, *102*, 271–284. https://doi.org/10.1111/cbdd.14238